

## A TWO-COMPONENT REFLECTION SEISMIC SURVEY, SPRINGBANK, ALBERTA<sup>1</sup>

DON C. LAWTON<sup>2</sup> AND MARK P. HARRISON<sup>2</sup>

### ABSTRACT

A converted-wave (*P-SV*) reflection seismic survey was recorded in conjunction with a conventional (*P-P*) survey over the eastern flank of the triangle zone near Springbank, in the Rocky Mountain foothills. The processed radial-component section is interpreted to contain reflections ranging from as deep as the Precambrian basement to very shallow reflectors in Tertiary rocks. Two *P-P* data sets were recorded, one using conventional 30-m geophone arrays and the other using the vertical component of single, 3-component geophones. After identical processing flows, both of these data sets resulted in comparable final sections. Static corrections for the radial-component data set are uncorrelated with those derived from the vertical-component data set. Residual shear-wave statics of up to 90 ms were calculated from the processing of the radial-component data. Reflections in the radial-component sections were enhanced considerably by the application of poststack *f-x* and *f-k* filters.

### INTRODUCTION

Recently, there has been increasing interest in multicomponent seismic data for providing an improved image of the subsurface (e.g., Domenico and Danbom, 1987; Frasier and Winterstein, 1990). In particular, the integrated interpretation of *P-P* and *P-SV* seismic sections may enable better estimates of lithological parameters (e.g., Poisson's ratio, density) to be made (Garotta et al., 1985). Over the past six years, the Geophysics Field School at the University of Calgary has been acquiring conventional *P*-wave reflection seismic data over the eastern limit of the fold and thrust belt of the Rocky Mountain foothills, west of Calgary. As part of the 1990 Field School, a 2-component reflection seismic program was undertaken to assess the applicability of a converted-wave (*P-SV*) survey in this area of mild subsurface structure.

In the study area (Twp 25, Rge 4 W5), and elsewhere along the eastern margin of the deformed belt, eastward-dipping Upper Cretaceous and Tertiary strata are juxtaposed

against westward-dipping, thrust rocks of Paleozoic to Tertiary age, which Gordy et al. (1977) have termed a *triangle zone*. Autochthonous rocks at depth form the base of the structure. Triangle zones in the Rocky Mountain foothills have since been discussed by Jones (1982), Teal (1983), McMechan (1985), Price (1986) and Charlesworth et al. (1987). The triangle zone developed as the result of the displacement of a wedge of sedimentary rocks into the foreland basin. The wedge is bounded by roof and sole thrust faults which Jones (1982) defined as the upper and lower detachments, respectively. The vergence of the sole thrust is foreland-directed, whereas that of the roof thrust is hinterland-directed. Tectonic delamination of the foreland succession occurs as the wedge is driven further into the basin. Sequences above the roof thrust are essentially autochthonous, except that they become uplifted as the wedging progresses.

Important gas fields occur in the western limb of the triangle zone (e.g., Turner Valley, Jumping Pound, Wildcat Hills), the reservoirs being located in carbonate rocks of Mississippian age in the hanging walls of major thrust faults. However, structural traps also occur in younger Mesozoic rocks within the triangle zone, such as in the Bearberry-Ricinus Cardium and Viking oil and gas field (Jones, 1989).

The 1990 University of Calgary Geophysics Field School seismic program was located at Springbank, about 30 km west of Calgary. Seismic data were collected along line FS90-1 (Figure 1), which is 3 km in length and is located on the eastern flank of the triangle zone near the Jumping Pound gas field. Figure 2 shows a generalized stratigraphic column of the study area, with the main seismic markers identified by arrows. Structures involved with the triangle zone in this region of the foothills are confined to the Upper Cretaceous Edmonton and Belly River Formations.

The objectives of the Field School program were to elucidate the eastward limit of triangle zone deformation and to

<sup>1</sup>Presented at the C.S.E.G. National Convention, Calgary, Alberta, May 15, 1991. Manuscript received by the Editor February 1, 1992; revised manuscript received April 1, 1992.

<sup>2</sup>Department of Geology and Geophysics, The University of Calgary, Calgary, Alberta T2N 1N4

The data were collected by staff and students participating in the 1990 University of Calgary Geophysics Field School and assisted by Eric Gallant of the CREWES Project. In particular, we thank Malcolm Bertram and Carl Gunhold for maintaining the field equipment and offering many helpful suggestions. All data processing was performed using Western Geophysical software operating on the CREWES Project IBM data processing facility. Support from the Natural Sciences and Engineering Research Council of Canada (NSERC) is also gratefully acknowledged. Useful comments on the manuscript were provided by three anonymous reviewers.

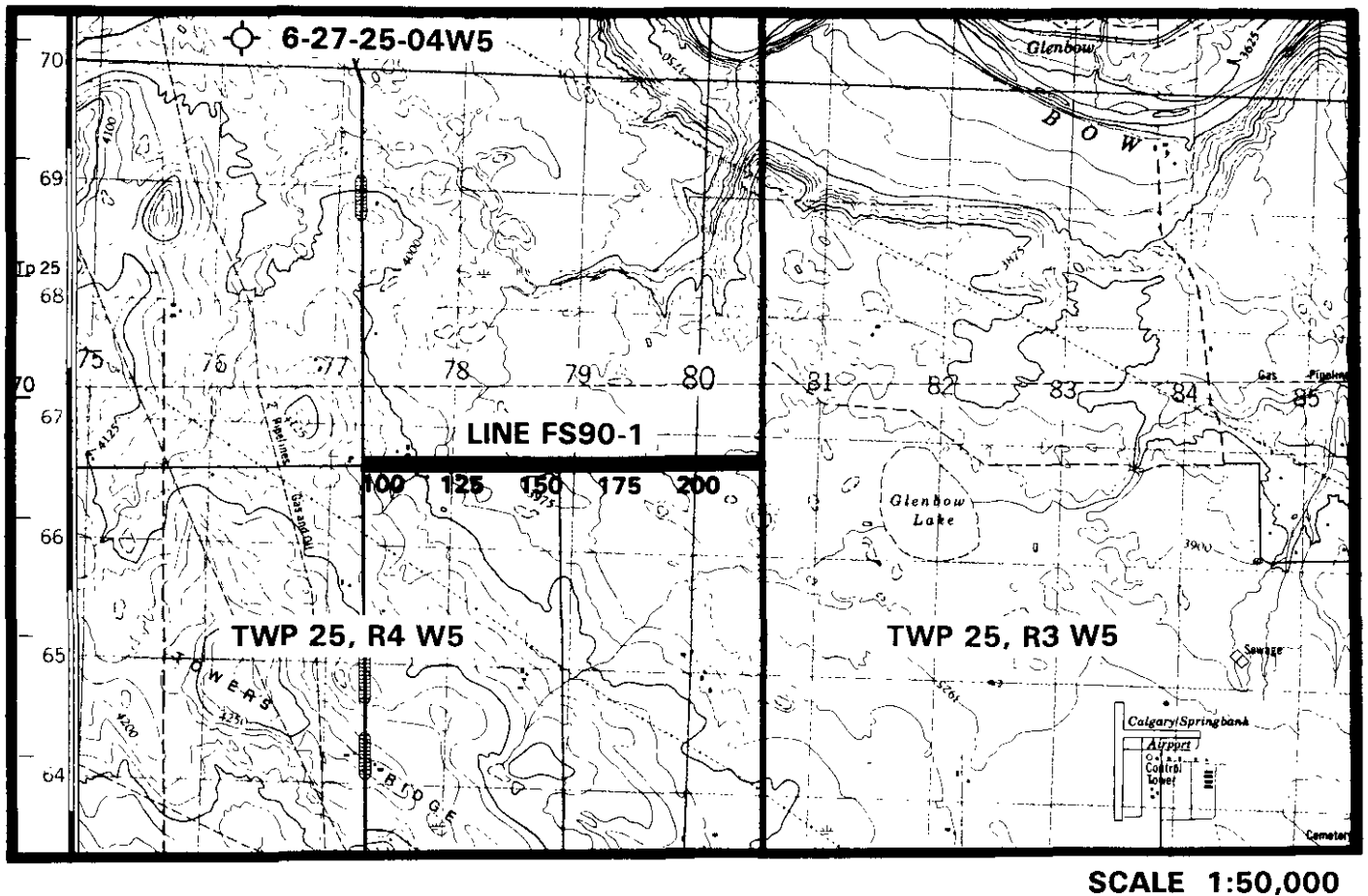


Fig. 1. Location map of the multicomponent seismic line FS90-1.

test the applicability of a converted-wave ( $P$ - $SV$ ) survey in an area with mild structure and gently dipping reflectors. These objectives were met by recording a conventional  $P$ -wave survey as well as a 2-component (radial and vertical) survey along line FS90-1. The conventional survey was recorded with the additional goal of enabling a comparison to be made between a  $P$ - $P$  seismic section acquired with geophone groups to one acquired with single geophones.

#### DATA ACQUISITION

All data were acquired using seismic equipment owned and operated by the Department of Geology and Geophysics, University of Calgary. The conventional  $P$ -wave survey was recorded with 48-channel DFS-III instruments and the 2-component survey was recorded with 96-channel Sercel 338HR instruments arranged in a 2x48 trace configuration. Hence, three separate 48-trace spreads were collected for each shot. For the multicomponent data, 2-component recording was favoured over 3-component recording because of the limited number of channels available and the desire to have at least 48 channels of radial component data.

The instruments were slaved together and a common energy source, consisting of 1 kg of dynamite, was loaded to

a depth of between 10 and 15 m at each shotpoint. This depth was chosen so that the dynamite was placed within a heavy clay layer, as this has been found to provide the most effective shot coupling. This clay layer is underlain by loose gravels which couple the shot energy poorly and are also difficult to drill through. Table 1 shows the acquisition parameters used in the survey. The geometry used was similar to that from previous Field School surveys (Slotboom et al., 1990) and is designed to provide for the optimum imaging of reflections in the first second of data. It was decided to use the same geometry for the 2-component survey as used for the conventional survey since modelling prior to the program showed that the amplitude of converted shear waves on the radial channel should be of the same order as the amplitude of compressional waves on the vertical channel over the mid to far source-receiver offset range. As an example, Figure 3 shows synthetic, NMO-corrected  $P$ - $P$  and  $P$ - $SV$  shot gathers based on the  $P$ -wave velocity structure in a well at 6-27-25-4W5. This well is located about 4.5 km northwest of the centre of line FS90-1 (Figure 1). The synthetic seismograms and stacks were generated using a method described by Howell et al. (1991). Since no shear wave velocity information was available, a constant Poisson's ratio of 0.30 was assumed for the entire depth interval, this value being typical for

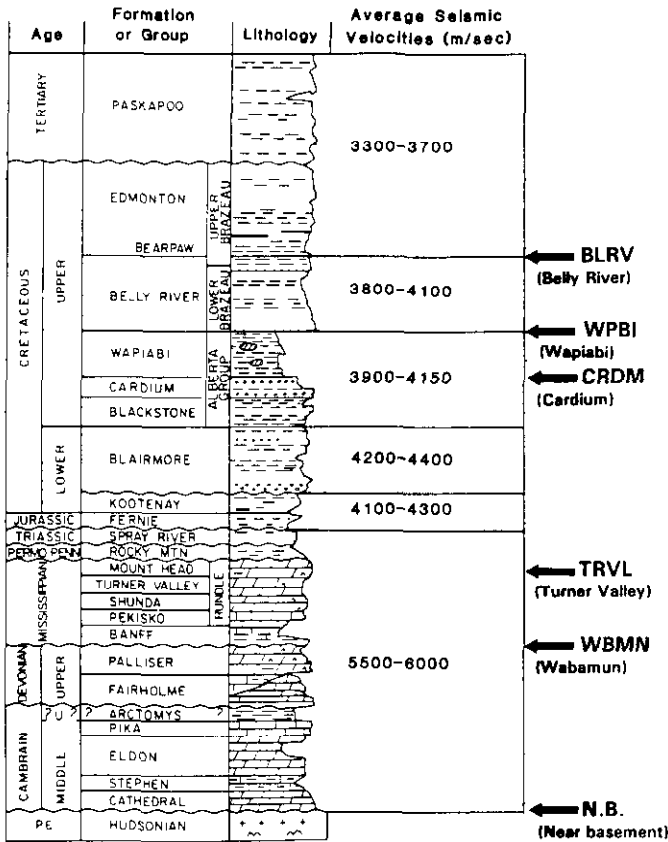


Fig. 2. Table of formations in the foothills west of Calgary (after Gallup, 1975, and Slotboom et al., 1990). The arrows indicate major seismic markers.

sedimentary rocks in the western Canada sedimentary basin (Miller and Stewart, 1990).

A near offset of 30 m was used for the survey in order to image the very shallow reflectors using both *P-P* and *P-SV* data. The nominal subsurface coverage was 24-fold, but the actual fold varied considerably because of the shortness of the line and the presence of a 400-m shot gap, due to the proximity of a water well to the line. For the conventional survey, recorded with the DFS III instruments, a low-cut filter of 12 Hz with a slope of 36dB/octave was employed as this had been used successfully in past surveys in the area (after considerable testing). The choice of low-cut filters in the Sercel instruments was debated after some test records had been acquired. It was preferred initially that a low-cut filter should not be used for acquiring *P-SV* data, but the high amplitudes of surface waves and multiple shear-wave refractions on the radial channel were of concern in terms of the available dynamic range of the instruments. After examination of the test records, we decided to use a 20-Hz low-cut filter but with a gentle slope of only 12 dB/octave.

Figure 4 shows an example of three common-shot records acquired during the survey. The conventional record (Figure 4a), acquired with geophone groups, has the highest signal-to-noise ratio across all channels. The record acquired with

Table 1. Field acquisition parameters.

Parameter	Conventional	2-component
Group interval	30 m	30 m
Shot interval	30 m	30 m
Shot size (common)	1 kg	1 kg
Shot depth (common)	10-15 m	10-15 m
Spread (end-on)	SP-30 m-1440 m, shot at east end.	
Geophones	M.P., 14 Hz	3-C Oyo, 10 Hz
Array	9 over 30 m	single
Instruments	DFS-III	Sercel 338HR
Channels	48	96
Low-cut filters	12/36	20/12
Notch (60 Hz)	in	in
Sample interval	2 ms	2 ms
Record length	4 s	6 s

single, vertical-component geophones (Figure 4b) shows surface wave energy which dominates reflections on traces over the near half of the record; the radial-component record (Figure 4c) is totally dominated by source-generated noise, with few reflections visible.

### DATA PROCESSING

The vertical (*P-P*) component of the 2-component data set was processed using the flow shown in Figure 5. A double-gated spiking deconvolution was applied, due to the length of the data window. The initial elevation and refraction statics solution produced a gradual delay of about 16 ms in reflection times of the deeper events near the west end of the line. This delay is greater than that expected from the regional westerly dip of the Precambrian basement in the study area, and was attributed to poor static control, and was removed using common source and common receiver stacks. The final section obtained is shown in Figure 6. To improve the signal-to-noise ratio, mainly in the shallow part of the section, an *f-x* prediction filter was applied to the unfiltered stack, followed by a mild *f-k* filter, band-pass filter, and gain. The resulting section is displayed in Figure 7. Prediction operators, seven points in length, designed on windows 500 ms long and 50 traces wide, were used in the *f-x* filtering process. The *f-k* filter was designed to attenuate events with dips of greater than 4 ms per trace by 6 dB. Most of the post-stack signal enhancement was achieved by application of the *f-x* filter.

The conventional data set was processed using the same deconvolution parameters, static solution and velocity functions as were used in the vertical-component data. The resulting section is shown in Figure 8. To facilitate comparison with the vertical-component section, *f-x* and *f-k* filters were also applied poststack (Figure 9). The interpretation shown on Figure 9 is discussed later in this paper. There is some residual noise remaining in the final sections (Figures 7 and 9), between SP 180 and SP 195 at 0.6 s reflection time. This is probably due to reduced fold proximal to dropped shots in this area because of the water well.

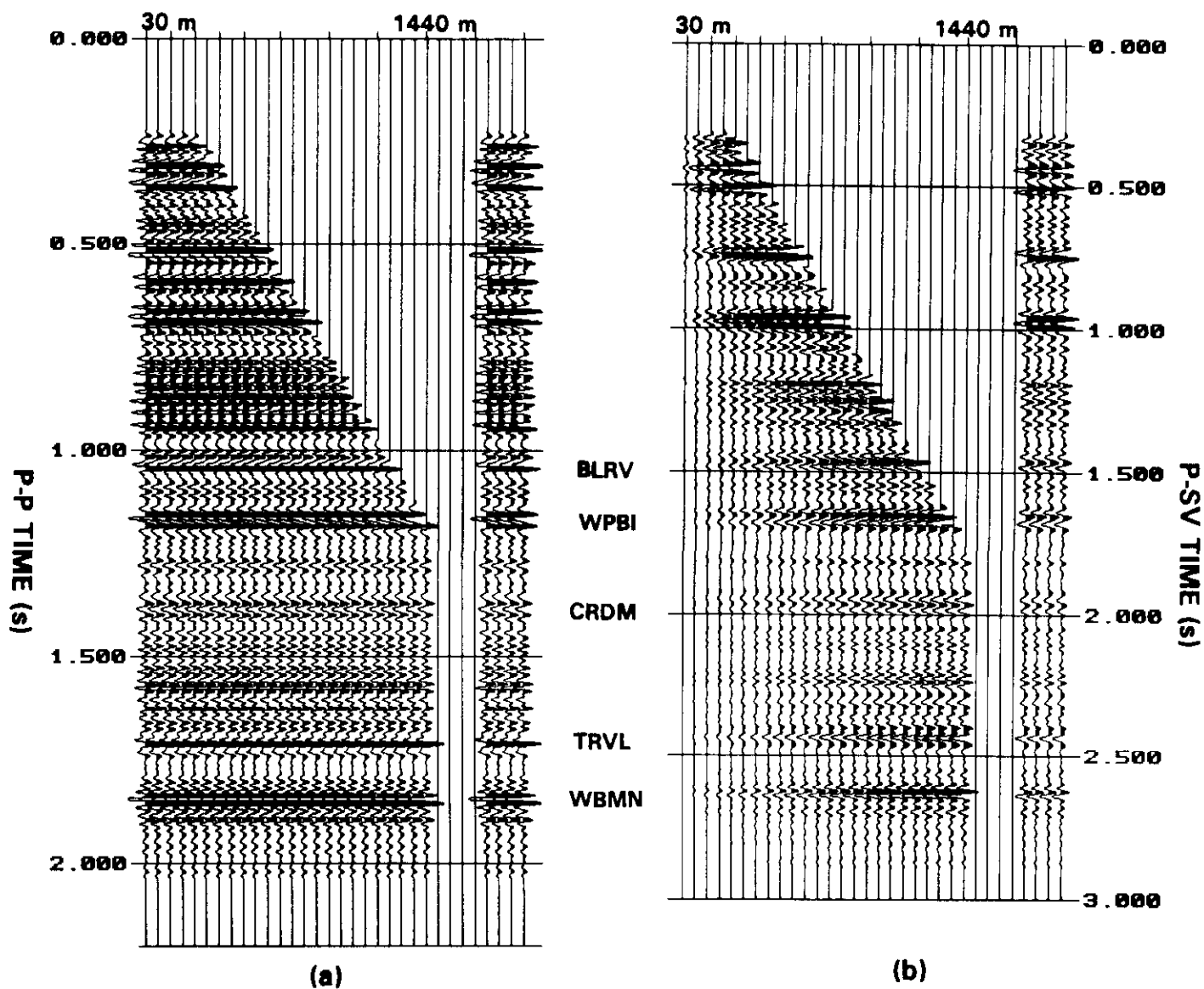


Fig. 3. Synthetic shot gathers with the same spread geometry used for the Field School Program: (a) *P-P*; (b) *P-SV*. The gathers were generated from a *P*-wave velocity model based on sonic log from well 6-27-25-4W5, and an assumed constant Poisson's ratio of 0.3.

The radial (*P-SV*) component data set was processed using the flow shown in Figure 10. Double-gated deconvolution was also applied to the *P-SV* data. The final statics solution from the vertical-component data was applied initially to the radial-component data. However, this static solution was found to be appropriate only for the source component of the statics solution, and residual receiver statics as large as 90 ms were obtained using common-receiver stacks. For this data set, there is no apparent correlation between the *P-P* and *P-SV* static solutions, as indicated from Figure 11, a result which is consistent with that discussed by Lawton (1990).

Estimates of  $V_p/V_s$  across various intervals were calculated by first correlating events between the *P-P* and *P-SV* stacked sections to get interval transit times, then using the formula:

$$V_p / V_s = \left( \frac{2I_s}{I_p} \right) - 1, \tag{1}$$

where  $I_p$  is the *P-P* time interval, and  $I_s$  is the *P-SV* time interval. The radial component data were then stacked using both the asymptotic approximation (Fromm et al., 1985), with  $V_p/V_s = 2.08$ , and also a more exact binning method, in which time-variant, common-conversion-point (CCP) gathers are assembled (Eaton et al., 1990). The stacked sections obtained using these two binning methods are shown in Figures 12 and 13, respectively, and the sections obtained after poststack *f-x* and *f-k* filtering are shown in Figures 14 and 15, respectively. The parameters used in applying the *f-x*

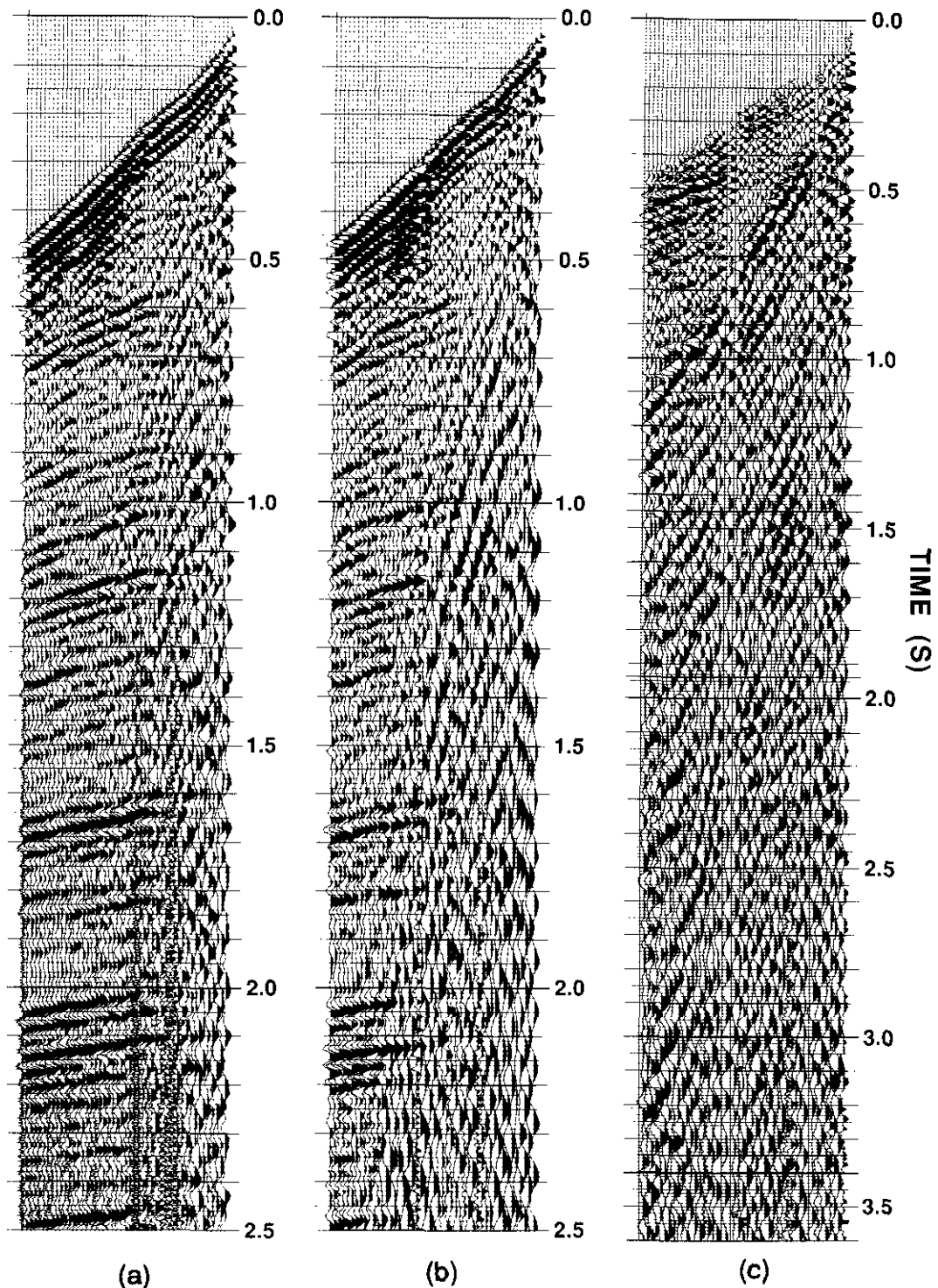


Fig. 4. Shot gathers from SP 161 of line FS90-1: (a) conventional; (b) vertical component; (c) radial component.

filter were identical to those used for the  $P$ - $P$  sections. The  $f$ - $k$  filter in this case was designed to attenuate events with dips greater than 4 ms per trace by 9 dB.

#### DISCUSSION

The band-pass-filtered sections of the vertical-component data (Figure 6) and the conventional data (Figure 8) are quite

similar, although the latter section contains slightly less random noise. Also of interest is the fact that the shallow data are better imaged on the conventional section than on the single-component section. It is usually expected that geophone arrays will smear shallow reflections and result in poorer stacked data than that obtained with point receivers. However, after the application of poststack  $f$ - $x$  and  $f$ - $k$  filters,

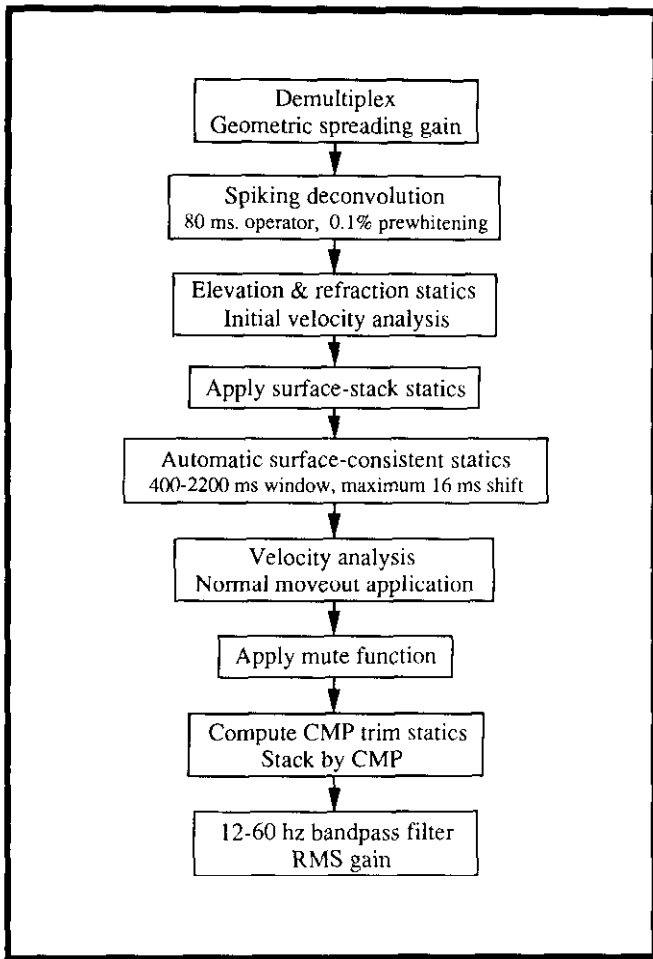


Fig. 5. Processing flow chart for the vertical-component ( $P$ - $P$ ) data.

both sections (Figures 7 and 9) are of comparable quality, although the shallow data are still more coherent in the conventional data (Figure 9). In comparison, band-pass-filtered sections of the radial-component data using both binning methods (Figures 12 and 13, respectively) contain a much higher level of noise than the vertical-component section (Figure 6). The origin of the noise is evident in common-offset stacks for the conventional ( $P$ - $P$ ), vertical-component ( $P$ - $P$ ) and radial-component ( $P$ - $SV$ ) data, shown in Figures 16a, 16b and 16c, respectively. Figures 16a and 16b are quite comparable, but the radial-component common-offset stack (Figure 16c) shows high-amplitude shot-generated noise which is visible at all offsets and overwhelms reflections over the near-half of the common-offset panel (source-receiver offsets of up to about 600 m). The origin and characteristics of this noise are discussed by Miller et al. (1990).

Figure 13 shows that depth-variant mapping of converted-wave data results in slightly better imaging of shallow reflections than the gathering and stacking of this type of data using an asymptotic approximation (Figure 12). The signal-to-noise ratio in both these  $P$ - $SV$  sections is improved substantially after the application of poststack  $f$ - $x$  and  $f$ - $k$  filters

(Figures 14 and 15). The quality of the data deteriorates towards the eastern (right) end of each section because of the decreasing offset range within each gather towards this end of the line.

## INTERPRETATION

Geological interpretations of the  $P$ - $P$  and  $P$ - $SV$  sections are shown in Figures 9 and 15, respectively. The main geological horizons (Figure 2) are identified and the upper and lower detachments of the triangle zone are imaged clearly on the  $P$ - $P$  data (Figure 9) by the change in reflector dip between times of 0.5 and 0.8 s. However, the upper detachment is not imaged very well by the  $P$ - $SV$  data (Figure 15), probably due to interference from shot-generated noise. In general, the eastern limit of triangle zone deformation is defined on both sections.

Most of the major  $P$ - $P$  reflections (Figure 9) can be correlated with  $P$ - $SV$  reflections (Figure 15). The sections are easier to compare if they are spliced together, as shown in Figure 17, and  $P$ - $P$  and  $P$ - $SV$  synthetic seismograms shown in the figure provide a useful means of correlating events between the two sections, at least at times greater than the reflection from the lower detachment. However, as evident in Figure 17, there are some significant differences in relative amplitudes between common events. For example, the Mississippian (TRVL) event is imaged slightly better on the  $P$ - $P$  section than on the  $P$ - $SV$  section, but the converse is true for the Cardium (CRDM) event. In future work we hope to determine whether these amplitude differences can be interpreted in terms of the petrophysical properties of these formations, or whether they are due to phase differences between the two data sets.

Another interesting aspect of the  $P$ - $SV$  section is that the interpreted near-basement event (3.2 s) is clearly defined by uniform amplitude and coherence, even though the maximum incident angle for a  $P$ - $SV$  raypath at this depth is calculated to be only about 10 degrees.

## CONCLUSIONS

This study has shown that reasonable quality  $P$ - $SV$  reflection data has been acquired in the Springbank area of Alberta, near the eastern limit of the triangle zone of the Rocky Mountain foothills. The converted-wave data were acquired in conjunction with production  $P$ - $P$  data, and identical recording geometries for the two types of surveys were used. In general, the amplitude of shot-generated noise on the radial-component data is significantly greater than that on the vertical-component data, and may overwhelm shear wave reflections over an offset range of about 600 m from the shot.

Key aspects of processing the converted-wave data were the calculation of shear wave static corrections separately from shot and receiver stacks, and the application of post-stack  $f$ - $x$  and  $f$ - $k$  filters to attenuate random and dipping noise. Final sections of similar quality were obtained from the conventional  $P$ -wave survey, which was recorded with a

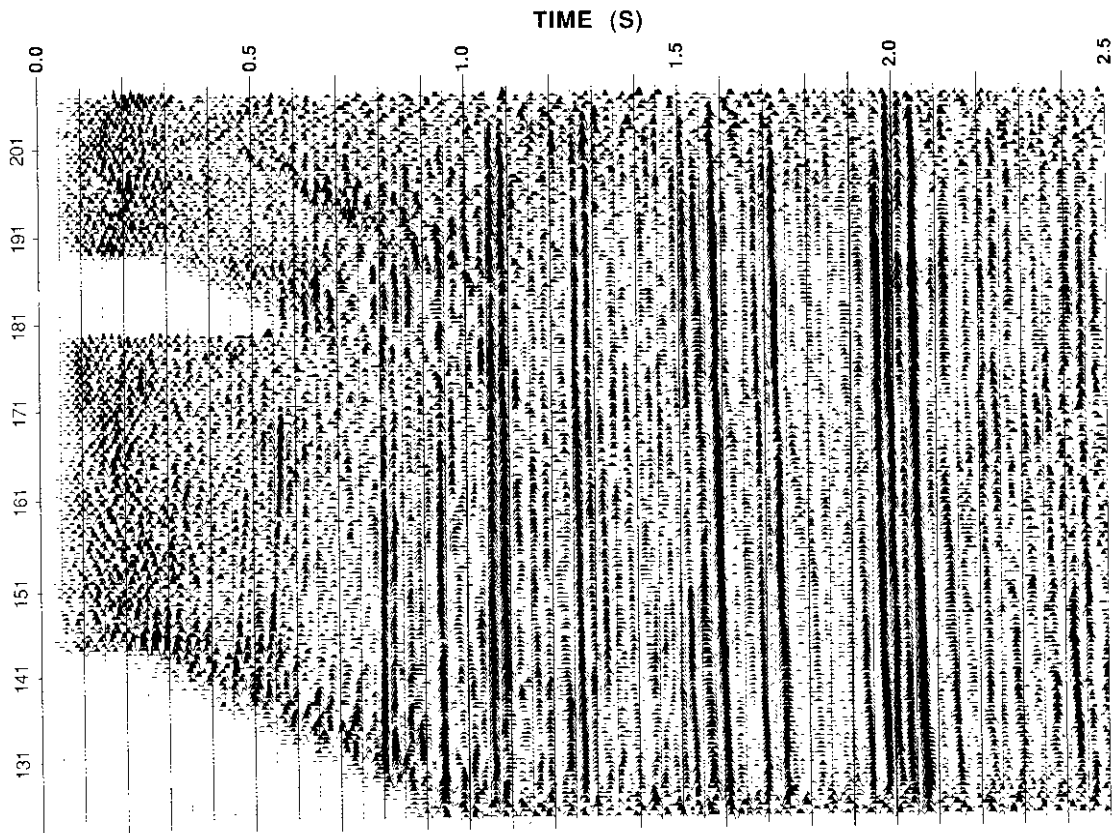
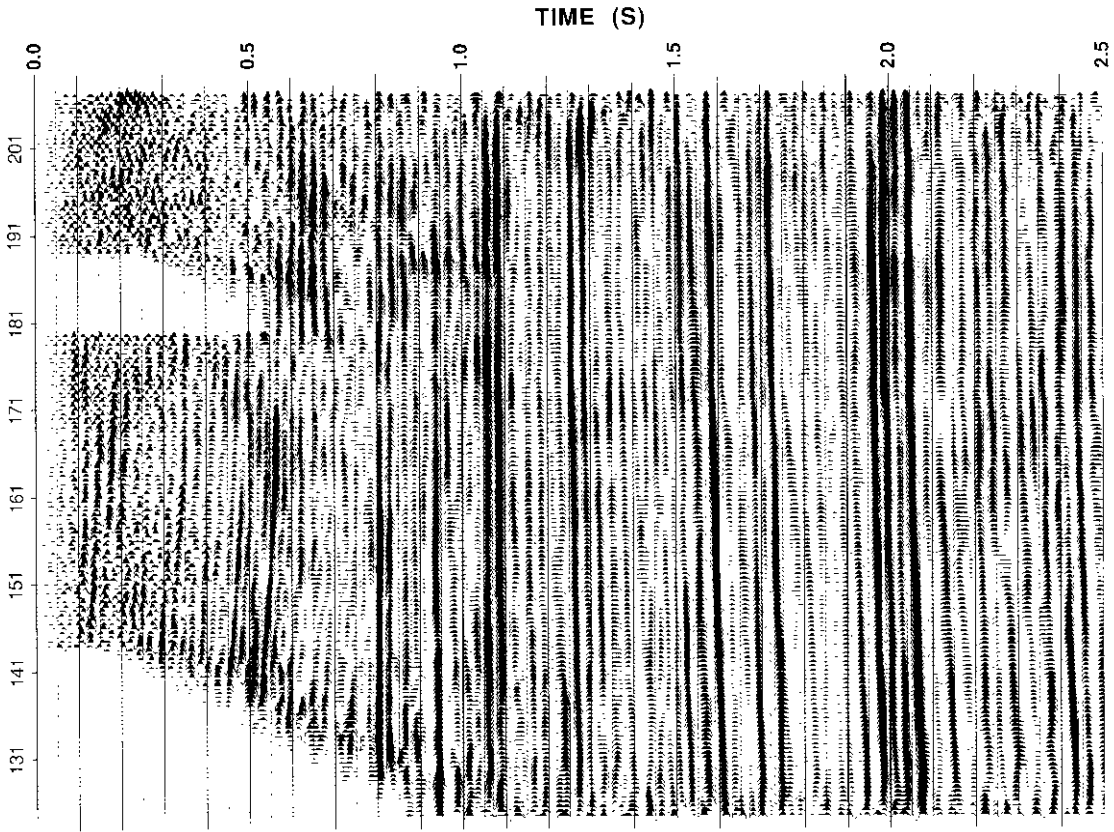


Fig. 6. Stacked section from single-geophone, vertical-component data.

Fig. 7. Stacked section from Figure 6 with poststack  $f_x$  and  $f_k$  filters applied.

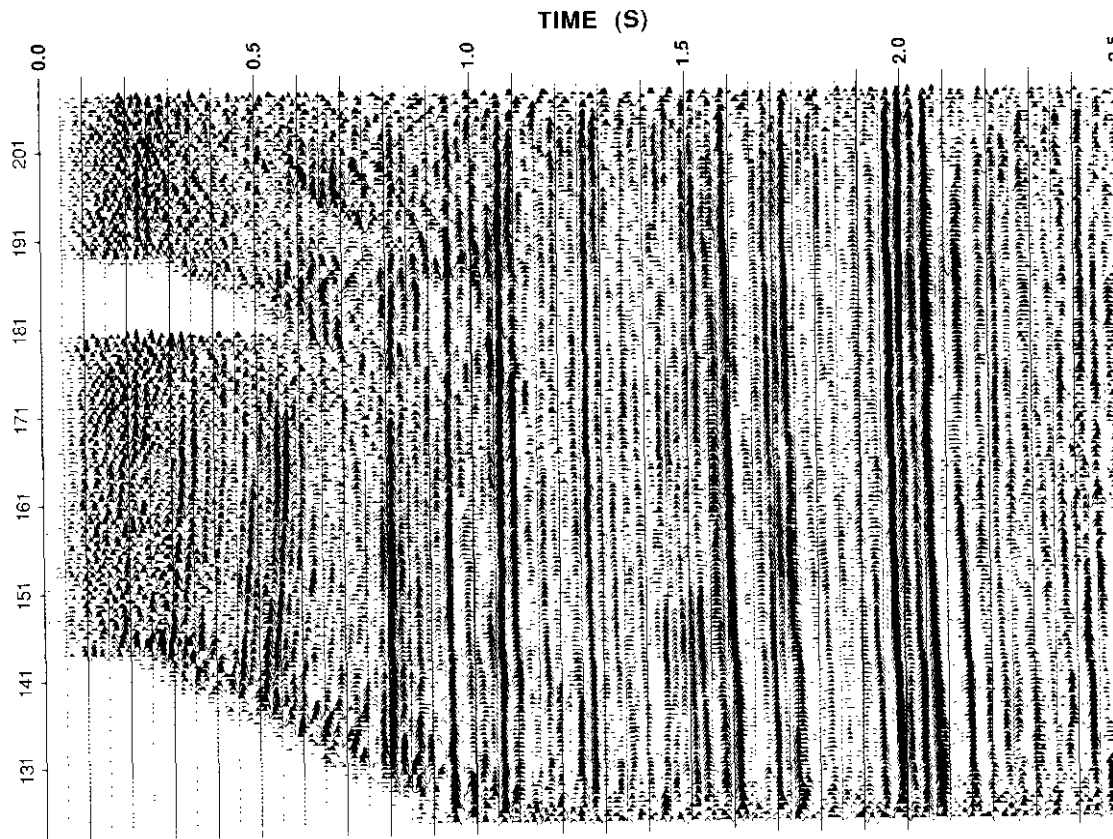
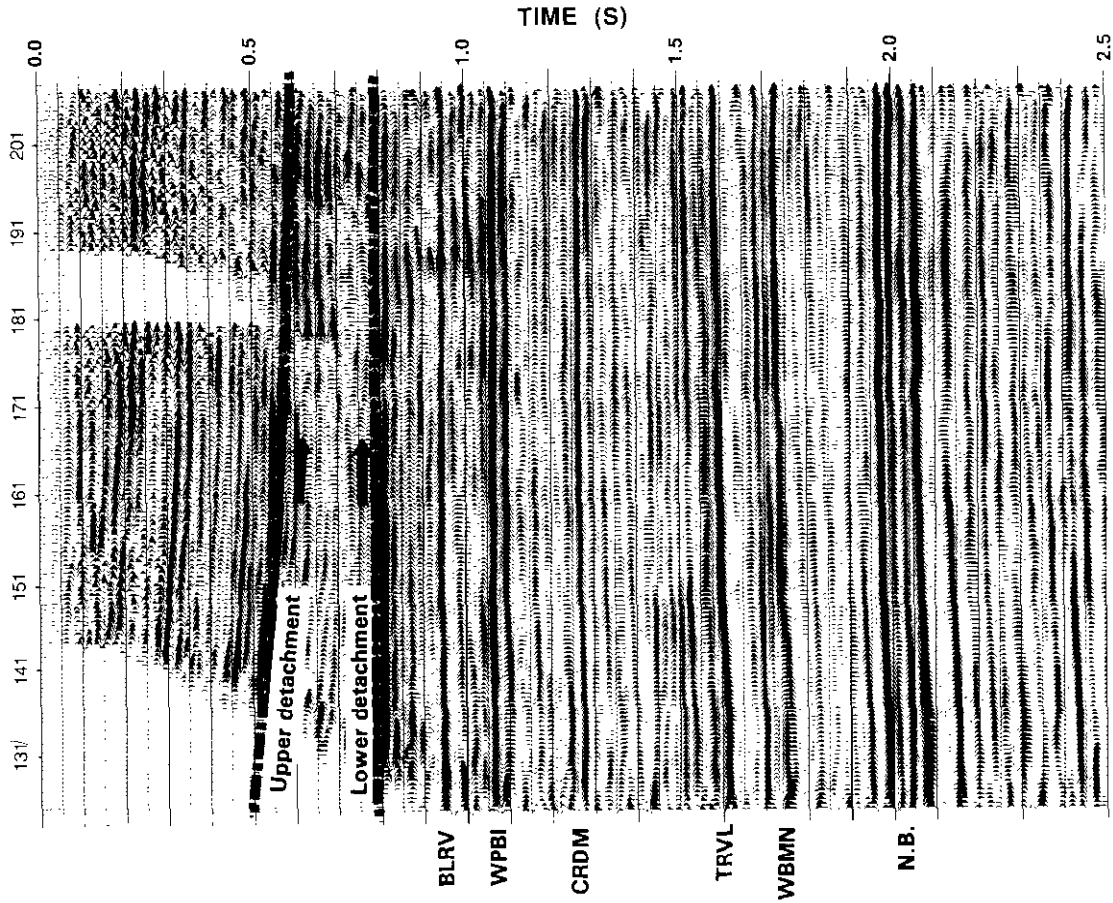


Fig. 8. Stacked section from conventional, vertical-component data.

Fig. 9. Stacked section from Figure 8 with poststack  $f_x$  and  $f_k$  filters applied. The interpreted positions of the upper and lower detachments are indicated, along with the major geological horizons from Figure 2.

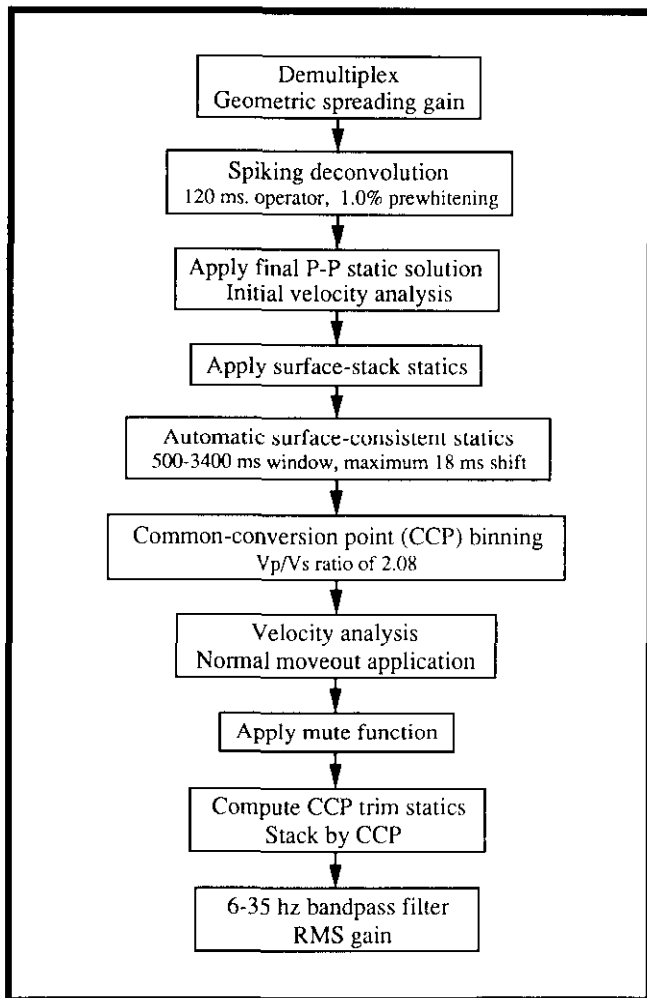


Fig. 10. Processing flow chart for the radial-component ( $P$ - $SV$ ) data.

30-m geophone array, and the vertical-component data, which was recorded with a single receiver at each station. However, the shallowest reflections exhibited better resolution in the former section.

Interpretation of the data showed that reflections from most of the major geological formation boundaries can be identified on both the  $P$ - $P$  and  $P$ - $SV$  sections, although there are significant differences in relative amplitudes between the two sections. Strong converted wave reflections from near-basement reflectors were recorded.

The most significant conclusion from this study is that  $P$ - $SV$  data can be acquired successfully during seismic surveys designed for conventional  $P$ - $P$  data acquisition.

## REFERENCES

- Charlesworth, H.A.K., Johnston, S.T. and Gagnon, L.G., 1987, Evolution of the triangle zone in the Rocky Mountain foothills of central Alberta: *Can. J. Earth Sci.* **24**, 1668-1678.
- Domenico, S.N. and Danbom, S.H., 1987, Shear-wave technology in petroleum exploration — past, current, and future, *in* Danbom, S.H. and Domenico, S.N., Eds., *Shear-wave exploration: Geophysical development series*, Vol. 1, Soc. Expl. Geophys., 3-18.
- Eaton, D.W.S., Slotboom, R.T., Stewart, R.R. and Lawton, D.C., 1990, Depth-variant converted wave mapping: Presented at the 1990 Nat. Conv., Can. Soc. Expl. Geophys., Calgary.
- Frasier, C. and Winterstein, D., 1990, Analysis of conventional and converted mode reflections at Putah Sink, California using three-component data: *Geophysics* **55**, 646-659.
- Fromm, G., Krey, T. and Wiest, B., 1985, Static and dynamic corrections, *in* Dohr, G., Ed., *Seismic shear waves: Handbook of geophysical exploration*, Vol. 15a, Geophysical Press, 191-225.
- Gallup, W.B., 1975, A brief history of the Turner Valley oil and gas field. *in* Foothills field trip guide book: CSPG/CSEG, 12-17.
- Garotta, R., Marechal, P. and Magneson, M., 1985, Two-component acquisition as a routine procedure for recording  $P$ -waves and converted waves: *J. Can. Soc. Expl. Geophys.* **21**, 40-53.
- Gordy, P.L., Frey, F.R. and Norris, D.K., 1977, Geological guide for the CSPG and the 1977 Waterton-Glacier Park Field Conference: *Can. Soc. Petr. Geol.*
- Harrison, M.P., 1989, Three-component seismic data processing: Carrot Creek, Alberta, *in* Stewart, R. R., Ed., *Consortium for research in elastic wave exploration seismology: Vol. 1*, Univ. of Calgary, 6-26.
- Howell, C.E., Lawton, D.C., Krebes, E.S. and Thurston, B., 1991,  $P$ - $SV$  and  $P$ - $P$  synthetic stacks, *in* Stewart, R.R., Ed., *Consortium for research in elastic wave exploration seismology: Vol. 3*, Univ. of Calgary, 191-204.
- Jones, P.B., 1982, Oil and gas beneath east-dipping underthrust faults in the Alberta foothills, *in* Powers, R.B., Ed., *Geological studies of the Cordilleran thrust belt: Rocky Mountain Assn. Geol. Bull.* **1**, 31-38.
- \_\_\_\_\_, 1989, Structural geology of the Alberta foothills front in the Calgary region, a field guide: International Tectonic Consultants Ltd.
- Lawton, D.C., 1990, A nine-component refraction seismic survey: *Can. J. Expl. Geophys.* **26**, 1-15.
- McMechan, M.E., 1985, *Low-taper triangle-zone geometry: an interpretation for the Rocky Mountain foothills, Pine Pass-Peace River area*, British Columbia: *Bull. Can. Petr. Geol.* **33**, 31-38.
- Miller, S.L. and Stewart, R.R., 1990, Effects of lithology, porosity and shaliness on  $P$ - and  $S$ -wave velocities from sonic logs: *Can. J. Expl. Geophys.* **26**, 94-103.
- \_\_\_\_\_, Bertram, M.B. and Lawton, D.C., 1990, Source-generated noise on multicomponent seismic data, *in* Stewart, R.R., Ed., *Consortium for research in elastic wave exploration seismology: Vol. 2*, Univ. of Calgary, 18-35.
- Price, R.A., 1986, The southeastern Canadian Cordillera: thrust faulting, tectonic wedging, and delamination of the lithosphere: *J. Struct. Geol.* **8**, 239-254.
- Slotboom, R.T., Lawton, D.C. and Spratt, D.A., 1990, The triangle zone in the Jumping Pound-Wildcat area, Alberta: Presented at the 1990 Nat. Conv., Can. Soc. Expl. Geophys., Calgary.
- Teal, P.R., 1983, The triangle zone at Cabin Creek, Alberta, *in* Bally, A.W., Ed., *Seismic expression of structural styles: Studies in geology, Series 15*, Am. Assn. Petr. Geol. **3**, 48-53.

A TWO-COMPONENT REFLECTION SEISMIC SURVEY

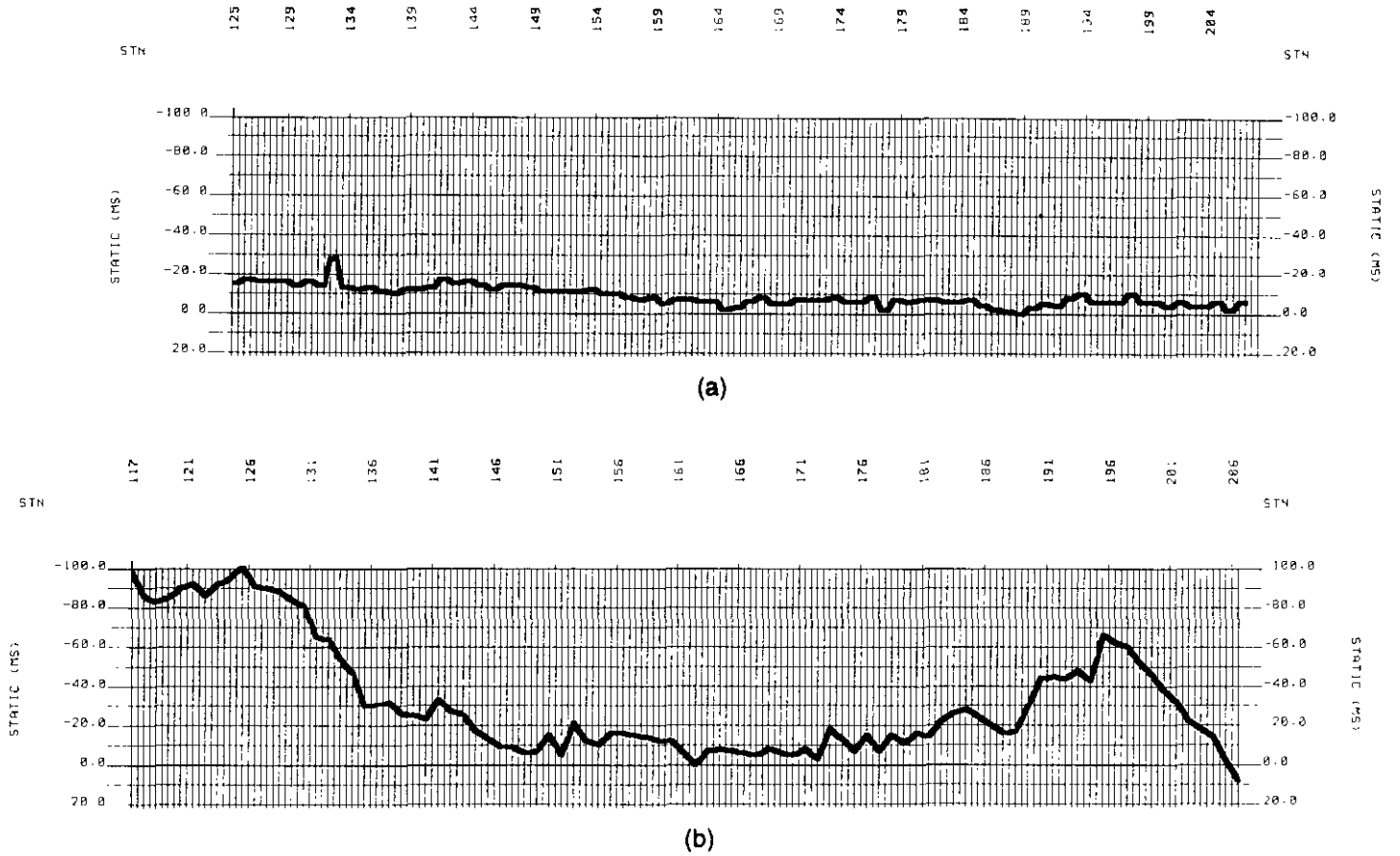


Fig. 11. Final static solutions for line FS90-1: (a) vertical component ( $P-P$ ); (b) radial component ( $P-SV$ ).

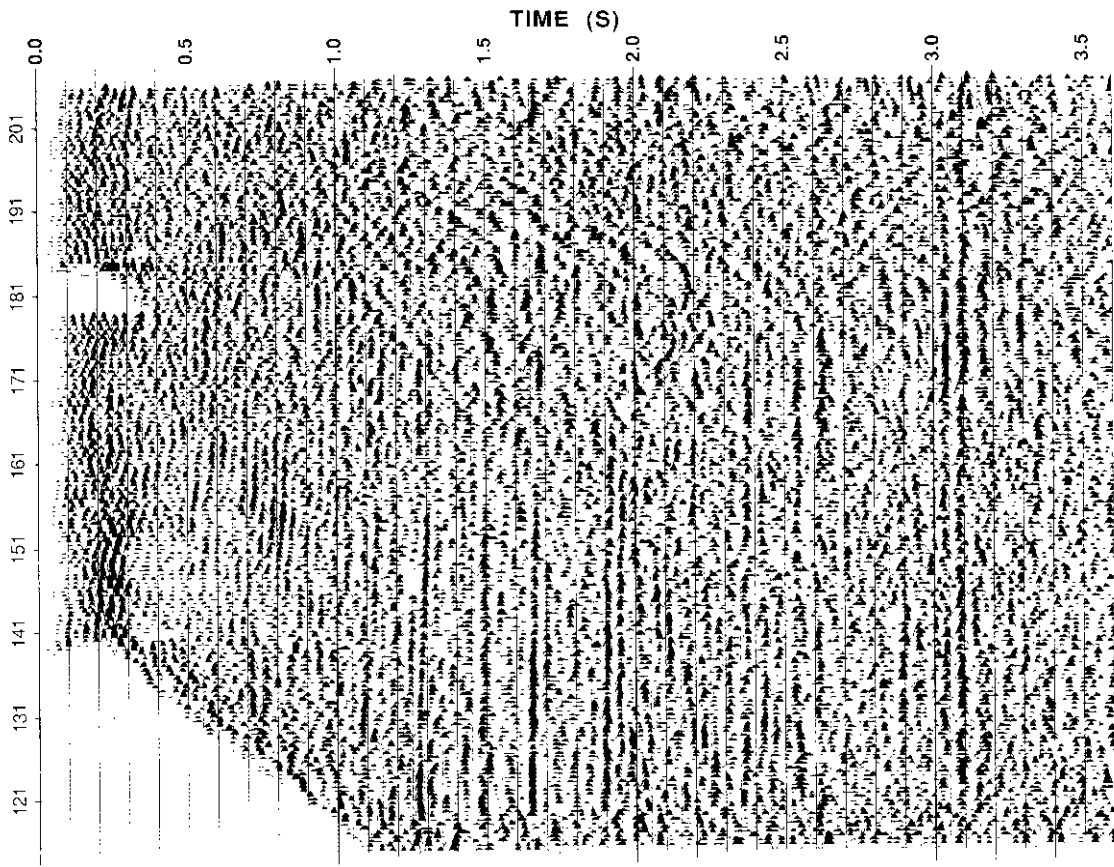


Fig. 13. Stacked section from single-geophone, radial-component data with depth-variant mapping.

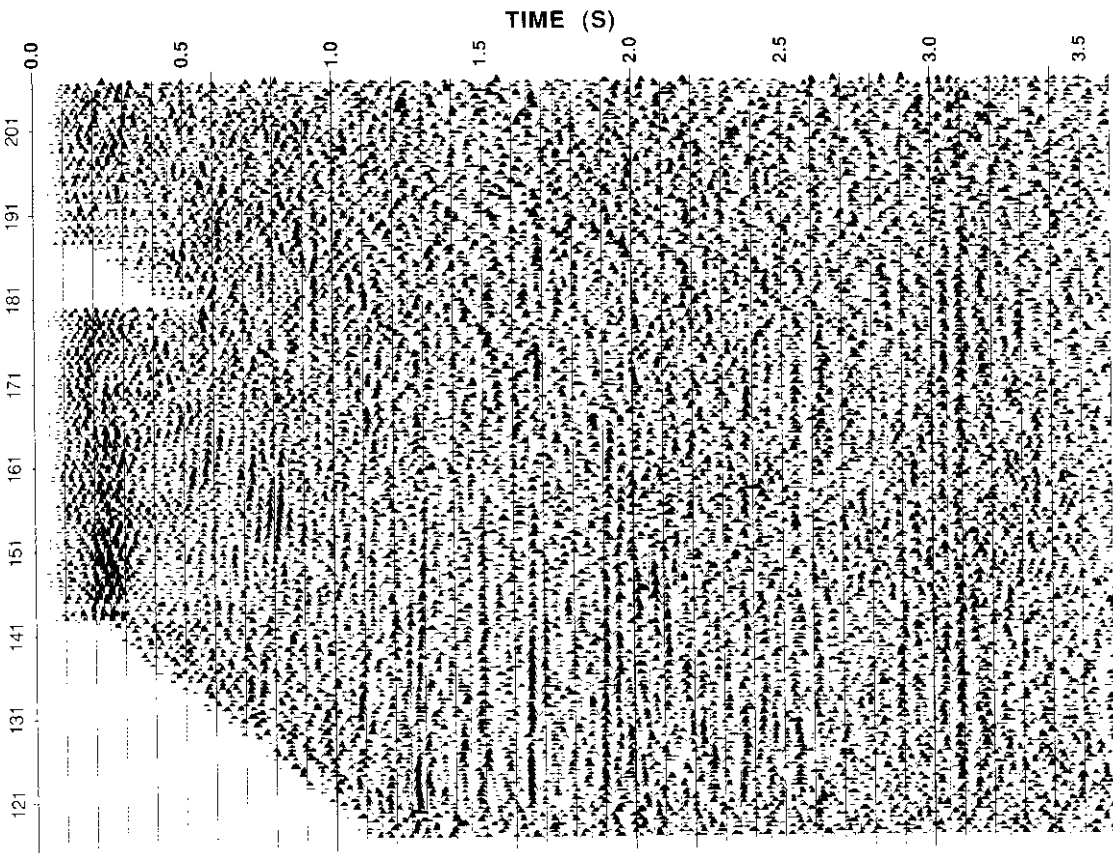


Fig. 12. Stacked section from single-geophone, radial-component data with asymptotic binning.

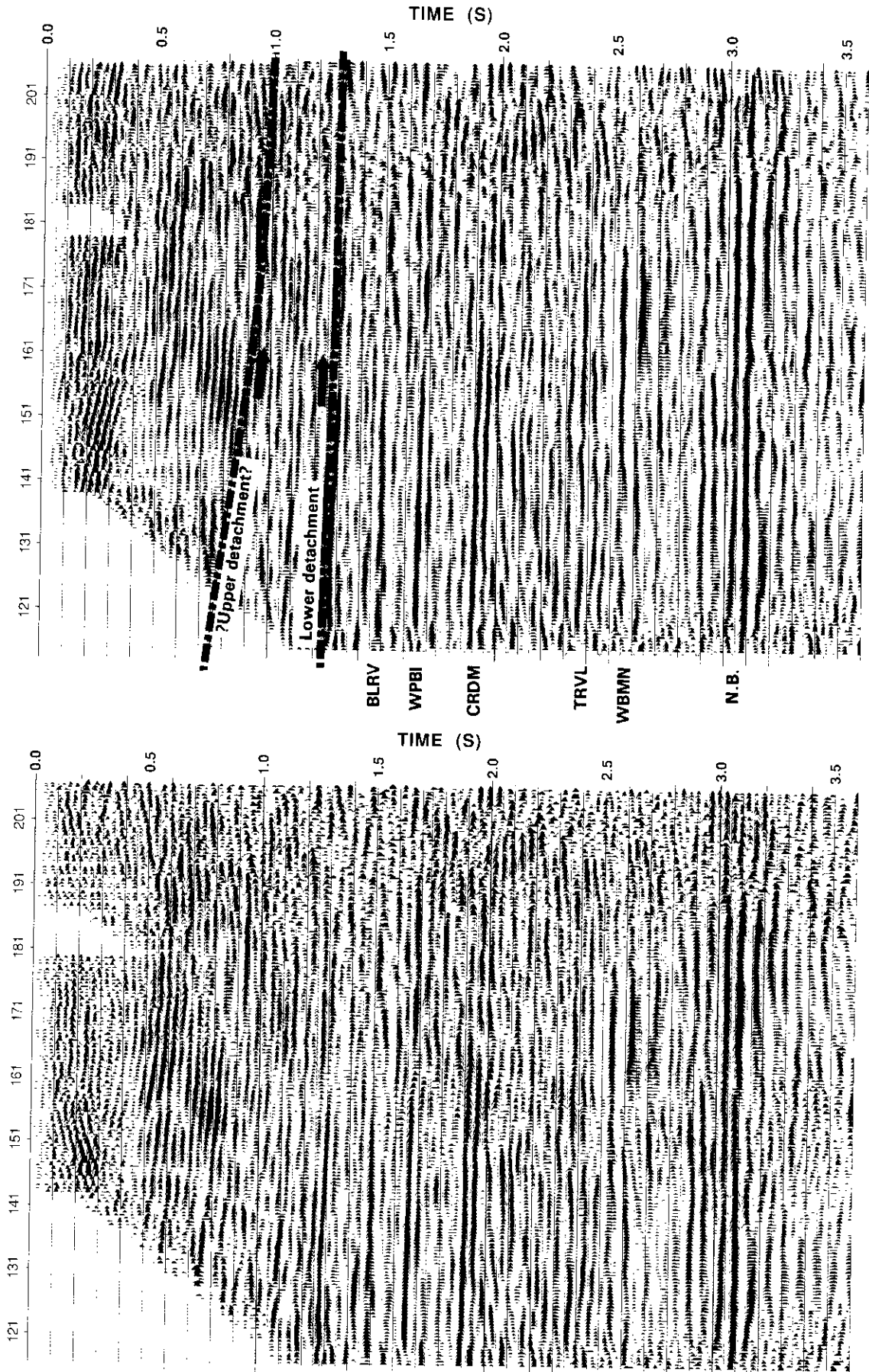


Fig. 14. Stacked section from Figure 12 with poststack  $f-x$  and  $f-k$  filters applied.

Fig. 15. Stacked section from Figure 13 with poststack  $f-x$  and  $f-k$  filters applied. The interpreted positions of the upper and lower detachments are indicated, along with the major geological horizons from Figure 2.

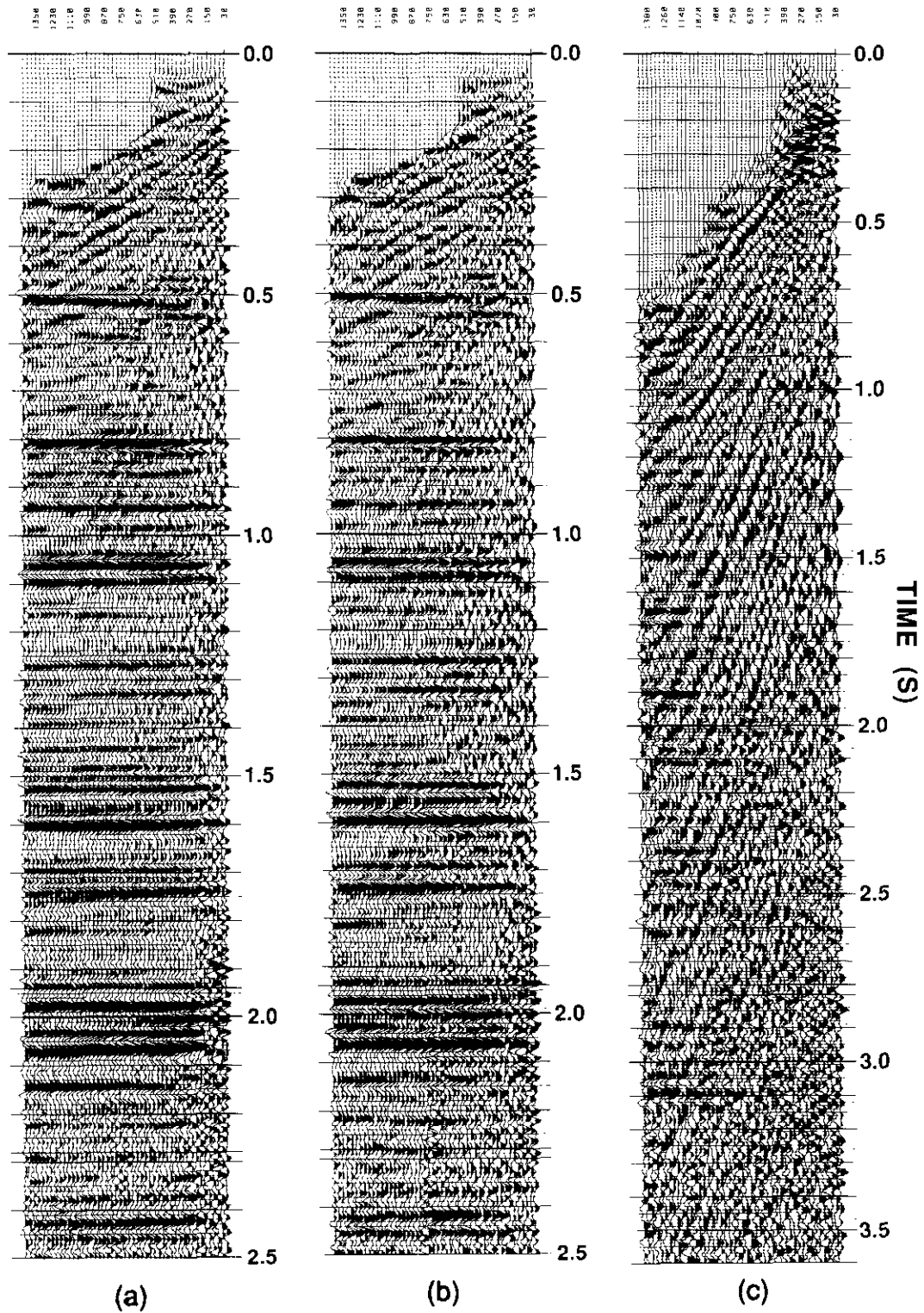


Fig. 16. Common-offset stacks from the central part of line FS90-1: (a) conventional; (b) vertical component; (c) radial component.

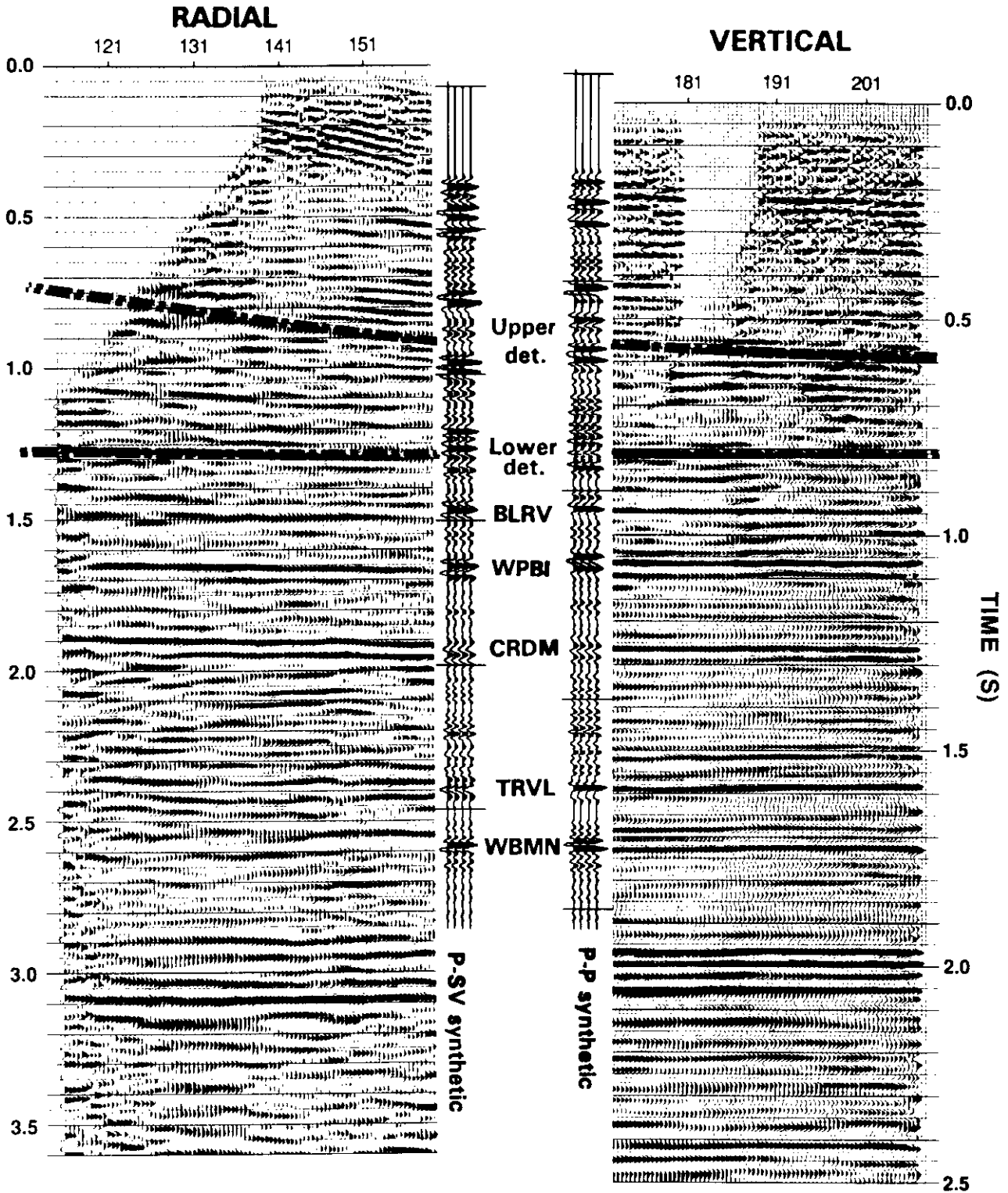


Fig. 17. Spliced *P-P* (vertical) and *P-SV* (radial) sections from Figures 9 and 15, showing correlation between the main events. Synthetic seismograms are based on a *P*-wave velocity model at well 6-27-25-4W5 and a ratio  $V_P/V_S = 2.08$ .